Extraction of Contact Resistance and DC Modeling in Metal Oxide TFTs

NA LI[1], WANLING DENG [1], XIXIONG WEI[1], WEIJING WU [2], AND JUNKAI HUANG[1]

1 Department of Electronic Engineering, Jinan University, Guangzhou 510630, China
2 State Key Laboratory of Luminescent Materials and Devices, South China University of Technology, Guangzhou 510640, China

CORRESPONDING AUTHOR: W. DENG (e-mail: dwanl@126.com)

ABSTRACT Based on the device physics, a simple and fast method of extracting contact resistance in metal oxide thin-film transistors (MOTFTs) is proposed through the *I–V* characteristics. This method divides the channel into two parts: the contact channel and the intrinsic channel, and assumes the electrons injected into the active layer at the source side are completed in the line injection. Using the *I–V* characteristics, the contact voltage can be obtained, and then the contact resistance can be extracted. The results indicate that contact resistance in MOTFTs depends on V_g, V_d, and L. Applying the extraction results, a dc drain current model considering contact resistance is proposed. Using this model, we can accurately describe the measurements of MOTFTs with channel lengths scaling from 50 μm to 10 μm. Through the extensive comparisons between the model results and the numerical iteration or experimental data, the validity of the method is strongly supported. This extraction method uses non-numerical iteration, which is simple, fast, and accurate.

INDEX TERMS Metal oxide thin-film transistors, contact resistance, contact voltage, dc model, *I-V* characteristics.

I. INTRODUCTION

Compared with amorphous silicon (a-Si), polysilicon (poly-Si) and organic thin film transistors, the metal oxide thin-film transistors (MOTFTs) have high carrier mobility, good uniformity and bending performance, low process temperature, and low cost deposition [1], [2]. Hence, MOTFTs have been found wide applications in the flexible circuits and active matrix organic light emitting diode (AMOLED) panels, etc. In the future applications, MOTFTs will also be applied to flexible Radio Frequency Identification (RFID) circuits [3], digital and mixed-signal circuits [4], biologically restorable biosensors and circuits [5], and so on. To improve the technology of MOTFTs, a full understanding of device physics in the oxide TFTs has become increasingly important.

As the device size continues to shrink, contact resistances in high-mobility and/or short channel TFTs seriously affect the device performance. It has a double detrimental effect. In other words, it reduces the effective gate-source overdrive, thus resulting in a lower channel accumulation, and

it also reduces the effective bias applied to the intrinsic drain-source channel [6], [7]. In some situations, the contact resistance may become comparable to, or even larger than, the channel resistance [8], [9]. Therefore, an accurate extraction of contact resistance plays an importance role in modelling, and makes us an in-depth understanding the device characteristics.

In the last few years, several extraction methods for a-IGZO TFTs have been proposed. Terada and Muta [10] and Chern *et al.* [11] first presented an approach to show the relationship between the total measured channel resistance and different mask channel lengths. Based on the approach, transmission line method (TLM) [12] was used to extract contact resistance. For a fixed gate voltage, the total resistance (R_T) shows a linear relationship with the channel length (L). By measuring the device characteristics at different L and by plotting R_T versus L, the contact resistance (R_c) can be extracted by a linear extrapolation of R_T-value for $L = 0$. However, the TLM method requires the measurements at

different L and is only valid in the linear mode at low V_{ds}. In addition, it assumes that R_c is independent on L, even though an explicit L-dependence of R_c is observed in practical a-IGZO TFTs [13]. It is important to note that, TLM is not allowed to extract R_c at high V_{ds}. Servati *et al.* [14] assumed a negligible contact resistance contribution for the long-channel transistors, but it was only valid in the linear regime. Considering any possible asymmetry in the S/D side, Ortiz-Conde *et al.* [15]–[17] and Raychaudhuri *et al.* [18] first independently put forward a simple method to extract the difference between the drain and source series resistance. Then Bae *et al.* [19] proposed a parallel-mode capacitance voltage (PMCV) technique for a separate extraction of R_S and R_D in individual a-IGZO TFTs. However, the relationships between R_c and other parameters such as L and V_{ds}, are not given in this method.

In this paper, we propose a physical-based straight forward extraction technique for contact resistance in MOTFTs. The channel is divided into the contact and the intrinsic parts [6], [20]. The line injection is assumed when the electrons are injected into the active layer at the source side. The method requires only two measurements, assuming that contact effects are negligible in the long channel transistors. Then, it can be applied to high V_{ds}. From the extraction of contact resistance, it is found that contact resistance in MOTFTs increases with the decrease of V_g, V_d, and L. By fitting the contact resistance for various conditions, an empirical model of R_c can be obtained. Combining the contact resistance with DC model, we can accurately describe the I-V characteristics of MOTFTs with channel lengths ranging from 50 μm to 10 μm.

II. EXTRACTION OF CONTACT RESISTANCE

In deriving the approach of extraction, an IZO TFT with staggered bottom gate structure is considered as an example, the structure diagram of which is given in Fig. 1. We introduce an assumption of zero potential at the back surface for the IZO active layer to obtain analytical model for the drain current. This assumption has its limitation for thin-body devices, but it is workable for modelling metal oxide TFTs [21].
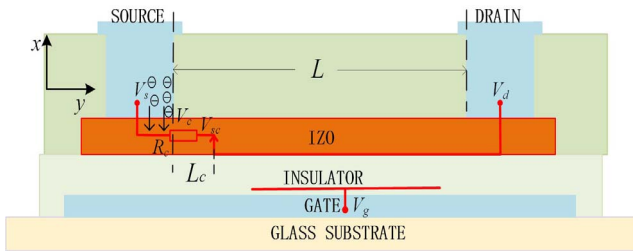

FIGURE 1. Cross section and electrical model of the staggered a-IZO TFTs.

As shown in Fig. 1, a general approach to analyze the contact characteristics is splitting the channel into two parts: a small contact region, where there is a voltage drop V_c (i.e.,

contact voltage), and the main channel, where the voltage drop is $V_d - V_c$ [6], [19]. Considering the contact effect, the drain current can be obtained as [22]

$$I_{ds} = -\frac{\mu_{eff}W}{L - L_c} \int_{V_c}^{V_d} Q_s d\phi_n \tag{1}$$

where μ_{eff} is the effective mobility, Q_s is the mobile charge density per unit area, ϕ_n is the channel potential, and L_c is the effective contact length actually contributing to the charge injection [6]. The contact length depends on the a-IZO thickness (T_s). When $T_s \leq 100$ nm, the contact length can be approximated as $L_c \approx 5T_s$ [7], [8]. Hence, the contact voltage V_c can be calculated by the numerical solution of (1).

In order to analytically solve the contact voltage, the charge-sheet model (CSM) is used to predict the drain current. For the extraction of contact resistance, the devices are restricted to operate in the turn-on region. Thus, assuming only the drift component is dominant, we can write the drain current as [23]

$$I_{ds} = -\mu_{eff}WQ_s\frac{d\varphi_s}{dy} \tag{2}$$

where φ_s is the surface potential. Integrating Eq. (2) under the boundary condition: $\varphi_{ss} = \varphi_s(y = 0)$ and $\varphi_{sd} = \varphi_s(y = L)$, the drain current can be obtained as

$$I_{ds} = \mu_{eff} \cdot C_{ox}\frac{W}{L} \cdot \left[\begin{array}{c} (V_g - V_{fb})(\varphi_{sd} - \varphi_{ss}) \\ -\frac{1}{2}(\varphi_{sd}^2 - \varphi_{ss}^2) - \frac{2}{3}\gamma\left(\varphi_{sd}^{3/2} - \varphi_{ss}^{3/2}\right) \end{array} \right] \tag{3}$$

where V_{fb} is the flat-band voltage, and $\gamma = (2\varepsilon_{izo}qN_b)^{0.5}/C_{ox}$ is the body factor. Note that (3) is valid for the intrinsic channel. If the contact effect is considered, similar to (1), Eq. (3) should be rewritten as

$$I_{ds} = \mu_{eff}C_{ox}\frac{W}{L - L_c} \cdot \left[\begin{array}{c} (V_g - V_{fb})(\varphi_{sd} - \varphi_{sc}) \\ -\frac{1}{2}(\varphi_{sd}^2 - \varphi_{sc}^2) - \frac{2}{3}\gamma\left(\varphi_{sd}^{3/2} - \varphi_{sc}^{3/2}\right) \end{array} \right] \tag{4}$$

where φ_{sc} is the surface potential at the contact side, i.e., $\varphi_{sc} = \varphi_s(y = L_c)$. Here, the surface potential at the contact side can be approximated as $\varphi_{sc} = \varphi_{ss} + V_c$, which matches well with the result in [23]. The contact voltage method also assumes the contact resistance can be ignored in the long-channel TFTs, as verified by the measurements in [24]. Therefore, for the long-channel transistors, drain current can be expressed by Eq. (3). Nevertheless, for the short-channel TFTs, drain current should be described by Eq. (4). Consequently, we define DI_d as

$$DI_d = \frac{I_{d\max}L_{\max}}{\mu_{eff}C_{ox}W} - \frac{I_{d\min}(L_{\min} - L_c)}{\mu_{eff}C_{ox}W} \tag{5}$$

where the subscripts "max" and "min" indicate the long- and short-channel devices, respectively.

Substituting Eqs. (3) and (4) into (5), we have

$$DI_d = \left[V_{gb}(\varphi_{sd} - \varphi_{ss}) - \frac{1}{2}\left(\varphi_{sd}^2 - \varphi_{ss}^2\right) - \frac{2}{3}\gamma\left(\varphi_{sd}^{3/2} - \varphi_{ss}^{3/2}\right) \right]$$

$$-\left[V_{gb}(\varphi_{sd}-\varphi_{sc})-\frac{1}{2}\left(\varphi_{sd}^2-\varphi_{sc}^2\right)-\frac{2}{3}\gamma\left(\varphi_{sd}^{3/2}-\varphi_{sc}^{3/2}\right)\right] \quad (6)$$

where $V_{gb}=V_g-V_{fb}$. Equation (6) can be rearranged as

$$DI_d = -\frac{1}{2}V_c^2 + \left(V_{gb}-\varphi_{ss}\right)V_c + \frac{2}{3}\gamma\left[\varphi_{ss}^{3/2}-(\varphi_{ss}+V_c)^{3/2}\right]. \quad (7)$$

Due to the complication of Eq. (7), we assume that

$$(\varphi_{ss}+V_c)^{3/2} \approx \alpha(\varphi_{ss}+V_c)+\beta(\varphi_{ss}+V_c)^2 \quad (8)$$

where the initial values of α and β are defined as 0.5. Substituting Eq. (8) into (7), the initial guess of V_{c0} can be obtained by solving the quadratic equation

$$AV_{c0}^2 + BV_{c0} + C = 0 \quad (9)$$

where $A=-0.5-\frac{2}{3}\gamma\beta$, $B=V_{gb}-\varphi_{ss}-\frac{2}{3}\gamma\alpha-\frac{4}{3}\gamma\beta\varphi_{ss}$, $C=\frac{2}{3}\gamma\varphi_{ss}^{1.5}-\frac{2}{3}\gamma\alpha\varphi_{ss}-\frac{2}{3}\gamma\beta\varphi_{ss}^2-DI_d$. Hence, V_{c0} can be acquired as

$$V_{c0} = \frac{-B+\sqrt{B^2-4AC}}{2A}. \quad (10)$$

To further improve the accuracy of the obtained contact voltage, the Schroder series can be introduced as

$$y_\omega = DI_d - \left\{-\frac{1}{2}V_c^2 + \left(V_{gb}-\varphi_{ss}\right)V_c \right.$$
$$\left. + \frac{2}{3}\gamma\left[\varphi_{ss}^{3/2}-(\varphi_{ss}+V_c)^{3/2}\right]\right\}. \quad (11)$$

Retaining the first two terms of the Schroder series, we can get the correction term ω as

$$\omega\left(y_\omega, y_\omega', y_\omega''\right) = \frac{y_\omega/y_\omega'}{1-0.5 y_\omega y_\omega''/\left(y_\omega'\right)^2} \quad (12)$$

where y_ω' and y_ω'' are the first and second derivatives of y_w versus V_c. As a consequence, a more accurate and complete contact voltage can be expressed as

$$V_c = V_{c0} + \omega\left(y_\omega, y_\omega', y_\omega''\right). \quad (13)$$

Therefore, the contact resistance R_c can be obtained by using $R_c = V_c/I_{ds}$ when V_c is extracted by (13).

III. DEVICE MODELING

For the MOTFTs, both the tail and deep trap states have great influence in a DC model [25], and the gate voltage V_g can push the Fermi level over the conduction band edge and both nondegenerate and degenerate transports are observed [26], [27]. A surface-potential-based DC model accounting for the charge transport in both nondegenerate and degenerate conduction regimes has been proposed in our previous work [28], i.e.,

$$I_{ds} = \left(1+MV_{deff}\right)\cdot\left[(1/I_{ab})^{m_2}+(1/I_{sub})^{m_2}\right]^{-\frac{1}{m_2}} \quad (14)$$

where M is a fitting parameter reflecting the slope of the output characteristics in the saturation region due to the

channel length modulation (CLM) effect [21], $V_{deff}=V_{ds}-(\varphi_{sd}-\varphi_{ss})$, and m_2 is a weight parameter. I_{ab} and I_{sub} are the drain currents in the accumulation and subthreshold regions, respectively, which can be expressed as [28]

$$I_{ab} = \frac{4\sqrt{2}q\mu_{eff}WN_c\phi_t C_{ox}}{LG_f\varepsilon_{izo}}\left[f_{ab}(\varphi_{sd})-f_{ab}(\varphi_{ss})\right] \quad (15)$$

$$I_{sub} \approx \frac{2\sqrt{2}q\mu_{eff}WN_c\phi_t C_{ox}^{\chi-1}\chi}{LG_t^{\chi/2}\varepsilon_{izo}^{\chi-1}(\chi-1)}\left[f_{sub}(\varphi_{sd})-f_{sub}(\varphi_{ss})\right] \quad (16)$$

where N_c is the effective density of states at E_c, $\phi_t = kT/q$ is the thermal voltage, $\chi = 2T_t/T$, $G_t = 2^{1+3T/2Tt}qg_c\theta_t\phi_t T_t/(\varepsilon_{izo}T)$, and $G_f = 2^{5/2}qN_c\theta_t/\varepsilon_{izo}$. Functions of $f_{ab}(\varphi_s)$ and $f_{sub}(\varphi_s)$ can be read by

$$f_{ab}(\varphi_s) = \left(\frac{\phi_t^2 C_{ox}^2}{\varepsilon_{izo}^2 G_f}-\frac{1}{2}\right)\left(V_{gb}-\varphi_s\right)^2+2\phi_t\varphi_s \quad (17)$$

$$f_{sub}(\varphi_s) = -\frac{1}{\chi}\left(V_{gb}-\varphi_s\right)^\chi+\frac{\phi_t^2\chi^2}{\chi-2}\left(V_{gb}-\varphi_s\right)^{\chi-2}. \quad (18)$$

The calculation of surface potential φ_s uses the high precision algorithm proposed by [28] considering the degenerate conduction. However, Eq. (14) does not include contact effects. For large carrier mobility and/or small channel lengths, the contact resistance may become comparable to, or even larger than, the channel resistance [8], [9]. As a result, the contact resistance must be considered in modelling. Including the contact resistance, (15) and (16) can be re-expressed as

$$I_{ab}^c = \frac{4\sqrt{2}q\mu_{eff}WN_c\phi_t C_{ox}}{(L-L_c)G_f\varepsilon_{izo}}\left[f_{ab}(\varphi_{sd})-f_{ab}(\varphi_{sc})\right] \quad (19)$$

$$I_{sub}^c \approx \frac{2\sqrt{2}q\mu_{eff}WN_c\phi_t C_{ox}^{\chi-1}\chi}{(L-L_c)G_t^{\chi/2}\varepsilon_{izo}^{\chi-1}(\chi-1)}\left[f_{sub}(\varphi_{sd})-f_{sub}(\varphi_{sc})\right]. \quad (20)$$

Herein, $\varphi_{sc} \approx \varphi_{ss} + V_c = \varphi_{ss} + R_c \cdot I_{ds}$. Therefore, the final drain current model can be acquired by substituting (19) and (20) into (14). This current expression can be applied to device modelling with different channel lengths.

IV. RESULTS AND DISCUSSIONS

As shown in Fig. 2, the transfer characteristics of a-IZO TFTs with different channel lengths were measured by Agilent B1500A. The fabrication process was similar to that of [29]. A 30 nm thick IZO film was deposited by RF magnetron sputtering, and the doping proportions of In$_2$O$_3$:ZnO were equaled to 1:1. The measured gate capacitance per unit area was $C_{ox} = 48.2$ nF/cm^2. The devices were fabricated with various channel lengths of 10, 15, 20, 30, 40, and 50 µm, and with channel width fixed to 100 µm. The measured a-IZO permittivity is $\varepsilon_{izo} = 11.5\varepsilon_0$, where ε_0 is the vacuum permittivity.

As indicated in Fig. 2, the normalized drain current ($I_{ds}L/W$) decreases as the channel length is decreased, representing a clear evidence of the increasing influence of contact
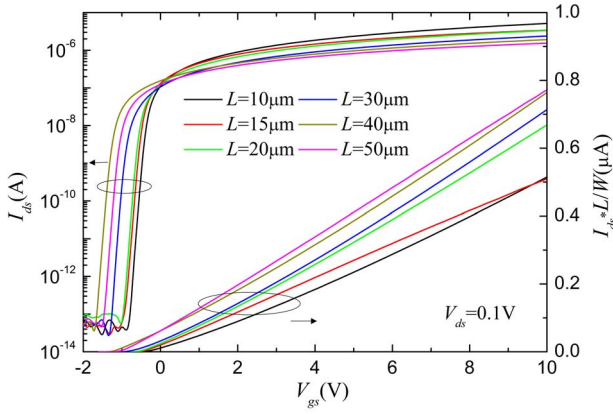
FIGURE 2. Transfer characteristics and normalized transfer characteristics of IZO-TFTs with different channel lengths.

FIGURE 4. Comparison of φ_{sc} solution between numerical results and approximation of $\varphi_{sc} = \varphi_{ss} + V_c$ with $V_{ds} = 0.1$ and 10.1 V.

effect on the short channel device characteristics. Here, we use the *I-V* characteristics of both long-channel ($L = 50$ μm) and short-channel ($L = 10$ μm) devices to get the value of *DId* according to (5). As a consequence, the contact voltage of a-IZO TFTs with $L = 10$ μm can be obtained by using (13). The comparison of the proposed contact voltage solution (13) versus numerical results is given in Fig. 3. The agreement with the numerical results is good.
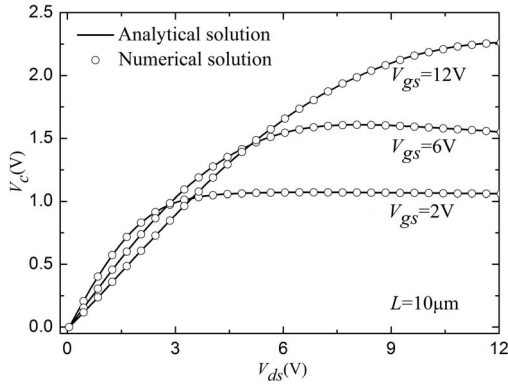

FIGURE 5. Contact resistance (black) and channel resistance (red) as a function of gate voltage with $V_d = 0.1$ V and $W/L = 100/10$ μm. Inset: Contact voltage (black) and intrinsic channel voltage (red) as a function of gate voltage in $V_d = 0.1$ V.

FIGURE 3. Comparison of analytical (lines) versus numerical (markers) contact voltage solutions.

In order to validate the approximation: $\varphi_{sc} = \varphi_{ss} + V_c$, the comparison of φ_{sc} solution between the numerical results and the approximation is demonstrated in Fig. 4. Obviously, the approximation agrees well with the numerical solution.

In the case of linear-injecting contacts, the total resistance R_T can be expressed as [12]

$$R_T = V_{ds}/I_{ds} = R_{ch} + R_c = r_{ch} \cdot L + R_c \quad (21)$$

where r_{ch} is the channel resistance per channel length unit.

Based on the results of Fig. 3 and the measurements of Fig. 2, the contact resistance R_c and channel resistance R_{ch} with $V_{ds} = 0.1$ V can be obtained, as shown in Fig. 5. As can be seen, the channel resistance R_{ch} and contact resistance R_c increase as the gate voltage V_g is decreased. The inset
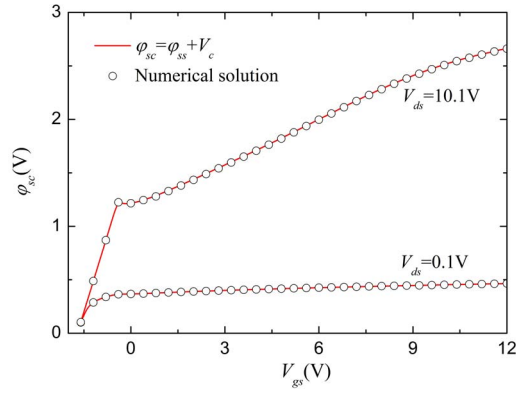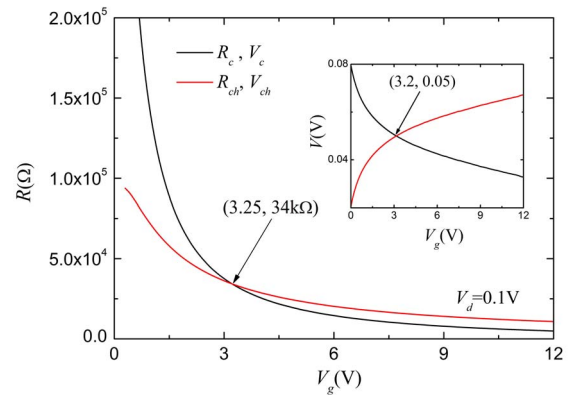
of Fig. 5 gives the results of V_{ch} and V_c, where V_{ch} is the intrinsic channel voltage (i.e., $V_{ch} = V_{ds} - V_c$). We can find that when $V_g \approx 3.25$ V, $R_c = R_{ch}$ and $V_c = V_{ch}$. When $V_g < 3.25$ V, the contact resistance R_c is larger than the channel resistance R_{ch} because $V_c > V_{ch}$. On the other hand, when $V_g > 3.25$ V, the condition of $V_c < V_{ch}$ results in R_c less than R_{ch}. Therefore, the contact resistance R_c has a greater influence on device performance in case of lower gate voltages.

In Fig. 6, the contact resistance of IZO-TFTs with $V_d = 0.1$ V is calculated by the proposed method, *I-V* characteristics method [6], and TLM [12], respectively. The good agreement confirms the effectiveness of the proposed approach.

As shown in Fig. 7 (a), the contact resistances with various channel lengths of 10, 20, and 30 μm are obtained under $V_d = 5.1$ V by using the proposed method. It can be seen that the contact resistance R_c increases as the channel length L is decreased. In Fig. 7(b), the contact resistances with $L = 15$ μm are extracted under $V_d = 2.6$, 7.6, and 10.1 V. As can be seen, R_c rises as the V_d is decreased.

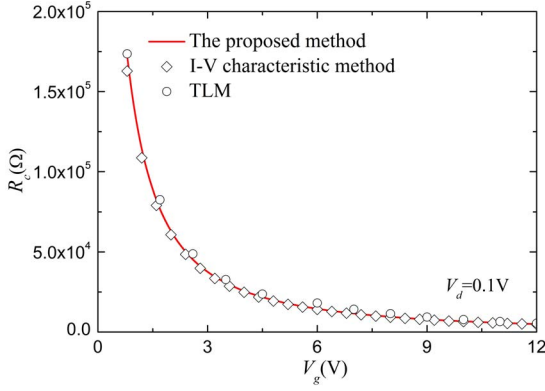**FIGURE 6.** Contact resistance as a function of gate voltage extracted by the *I-V* characteristic method [6], TLM [12], and our method.
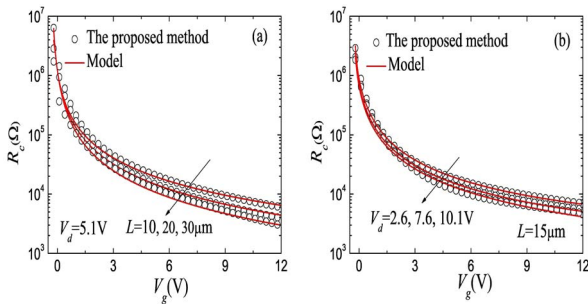

FIGURE 7. Contact resistance as a function of gate voltage with (a) various channel lengths of 10, 20, and 30 μm, and (b) V_d = 2.6, 7.6, and 10.1 V.
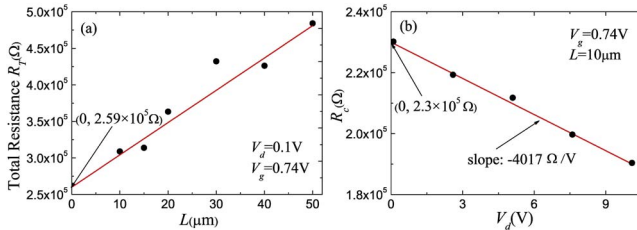

FIGURE 8. Extractions of (a) β by using TLM and (b) R_i and α.

The above results indicate that the contact resistance R_c in IZO-TFTs depends on V_g, V_d, and L [13]. Based on the extraction results, the contact resistance R_c can be empirically modelled as

$$R_c = (1 - \alpha \cdot L)(\beta - R_i \cdot V_d) \cdot \frac{1}{(V_g - V_T)^{1.2 + \alpha \cdot L}} \quad (22)$$

where V_T is the threshold voltage, R_i, α and β are the fitting parameters. The threshold voltage can be extracted as $V_T = -0.26$V by the linear extrapolation method [23].

From the Eq. (22), we can find that when V_d and L are very small, the value of β can be approximated as the resistance intercept of the plot of R_T vs. L with $V_g = V_T + 1$. Herein, R_T can be extracted by TLM. As shown in Fig. 8(a), we can observe that $\beta = 2.59 \times 10^5 \Omega V^{1.2+aL}$. Analogously, the parameters α and R_i can be respectively estimated by the

FIGURE 9. Comparisons of (a) transfer and (b) output characteristics between the model results (lines) and the measured data (markers) with $W/L = 100/50$ μm.

TABLE 1. Simulation parameters used in Figs. 9-11.

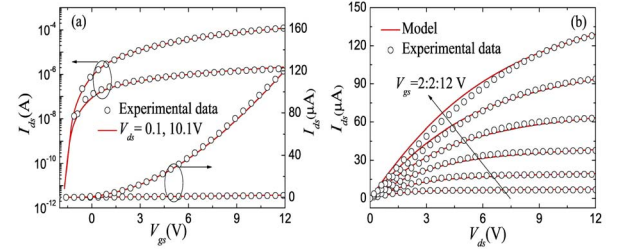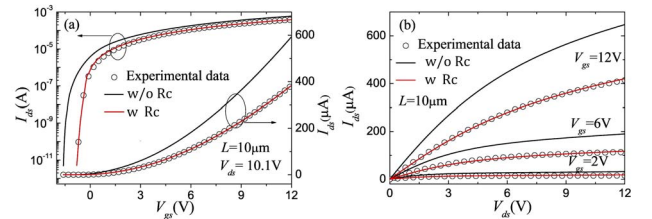| Parameter	Value	Parameter	Value	Parameter	Value
N_c (cm^{-3}eV^{-1})	5×10^{18}	kT (meV)	26	C_{ox}(nF/cm^2)	48.2
g_c (cm^{-3}eV^{-1})	4×10^{18}	kT_t (meV)	31	m_2(-)	2
k_1(cm^{2}s^{-1}V$^{-1-\lambda_1}$)	2.98	ϕ_{f0} (V)	-0.35	λ_1(-)	1.34
k_2(cm^{2}s^{-1}V$^{-1-\lambda_2}$)	7.5	V_{fb} (V)	-1.72	λ_2(-)	0.3

FIGURE 10. Comparisons of (a) transfer and (b) output characteristics between the model results (lines) and the measured data (markers) with $W/L = 100/10$ μm.

intercept and slope of the line of R_c vs. V_d with $V_g = V_T + 1$. The extracted process is shown in Fig. 8 (b), and the results after optimization are given as follows: $\alpha = 0.01$ μm^{-1} and $R_i = 5080\Omega V^{0.2+aL}$. Using these values, back to Fig. 7, we can see that the model and the extraction results are in a good agreement.

Figure 9 shows the model of Eq. (14) accurately predicts the measured transfer and output characteristics of the long channel a-IZO TFTs in a wide range of biases. The physical parameters are given in Table 1 [30].

However, as depicted in Fig. 10 of black lines, the model results of Eq. (14) overestimate the drain current in short channel a-IZO TFTs, and this can be ascribed to the limited charge injection at the source contact [7], [8], [31]. Therefore, in short channel a-IZO TFTs, the contact resistance must be considered in modelling. Substituting (22) with the contact resistance parameters extracted from Fig. 8, the drain current model with contact resistance can be obtained, which fits measurements well. It indicates that the extraction of contact resistance from the proposed method is useful to characterize MOTFTs.
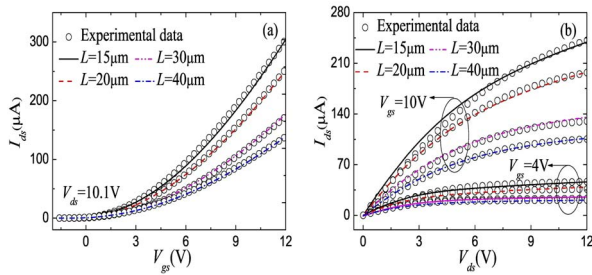
FIGURE 11. Comparisons of (a) transfer and (b) output characteristics between the model results (lines) and measured data (markers) with $L = 15, 20, 30, 40 \, \mu m$.

When the channel length varies, the final drain current model considering the contact resistance can accurately predict the measurements in Fig. 11, with the same set of parameters.

V. CONCLUSION

In this paper, we present a straight-forward and physical-based method to extract contact resistance. The extraction has important features. First, the contact voltage V_c at the source side is calculated, and thus, the contact resistance R_c can be analytically obtained. Second, from the extraction results, we find that the contact resistance depends on V_g, V_d, and L. The nonlinear relationship can be empirically modelled for fitting the behavior of contact resistance with various bias conditions. Lastly, the drain current model considering contact resistance is proposed, which accurately and consistently describes the measurements of MOTFTs with different channel lengths, using the same group of parameters.

REFERENCES

[1] K. Nomura *et al.*, "Room-temperature fabrication of transparent flexible thin-film transistors using amorphous oxide semiconductors," *Nature*, vol. 432, no. 4016, pp. 488–492, Nov. 2004.

[2] X. Yu, T. J. Marks, and A. Facchetti, "Metal oxides for optoelectronic applications," *Nat. Mater.*, vol. 15, no. 4, pp. 383–396, Apr. 2016.

[3] H. Ozaki, T. Kawamura, H. Wakana, T. Yamazoe, and H. Uchiyama, "Wireless operations for 13.56-MHz band RFID tag using amorphous oxide TFTs," *IEICE Electron. Exp.*, vol. 8, no. 4, pp. 225–231, Feb. 2011.

[4] D. Raiteri *et al.*, "A 6b 10MS/s current-steering DAC manufactured with amorphous gallium-indium-zinc-oxide TFTs achieving SFDR > 30dB up to 300kHz," in *IEEE Solid-State Circuits Conf. Dig. Tech. Papers*, vol. 55, 2012, pp. 314–316.

[5] D. H. Kim *et al.*, "Dissolvable films of silk fibroin for ultrathin conformal bio-integrated electronics," *Nat. Mater.*, vol. 9, no. 6, pp. 511–517, Jun. 2010.

[6] F. Torricelli *et al.*, "Transport physics and device modeling of zinc oxide thin-film transistors—Part II: Contact resistance in short channel devices," *IEEE Trans. Electron Devices*, vol. 58, no. 9, pp. 3025–3033, Sep. 2011.

[7] M. Ghittorelli *et al.*, "Unified physical DC model of staggered amorphous InGaZnO transistors," *IEEE Trans. Electron Devices*, vol. 64, no. 3, pp. 1076–1082, Mar. 2017.

[8] W. Wang *et al.*, "Analysis of the contact resistance in amorphous InGaZnO thin film transistors," *Appl. Phys. Lett.*, vol. 107, no. 6, pp. 1–4, Aug. 2015.

[9] R. I. Kondratyuk *et al.*, "A study of parasitic series resistance components in In-Ga-Zn-oxide (a-IGZO) thin-film transistors," *IEEE Electron Device Lett.*, vol. 32, no. 4, pp. 503–505, Apr. 2011.

[10] K. Terada and H. Muta, "A new method to determine effective MOSFET channel length," *Jpn. J. Appl. Phys.*, vol. 18, no. 5, pp. 953–959, May 1979.

[11] J. G. J. Chern, P. Chang, R. F. Motta, and N. Godinho, "A new method to determine MOSFET channel length," *IEEE Electron Device Lett.*, vol. EDL-1, no. 9, pp. 170–173, Sep. 1980.

[12] S. Martin *et al.*, "Influence of the amorphous silicon thickness on top gate thin-film transistor electrical performances," *Jpn. J. Appl. Phys.*, vol. 40, no. 2A, pp. 530–537, Feb. 2001.

[13] J.-H. Park *et al.*, "Empirical modeling and extraction of parasitic resistance in amorphous indium-gallium-zinc oxide thin-film transistors," *IEEE Trans. Electron Devices*, vol. 58, no. 8, pp. 2796–2799, Aug. 2011.

[14] P. Servati, D. Striakhilev, and A. Nathan, "Above-threshold parameter extraction and modeling for amorphous silicon thin-film transistors," *IEEE Trans. Electron Devices*, vol. 50, no. 11, pp. 2227–2235, Nov. 2003.

[15] A. Ortiz-Conde, J. J. Liou, W. Wong, and F. J. García-Sánchez, "A simple method to extract the difference of the drain and source series resistances in MOSFETs," *Electron. Lett.*, vol. 30, no. 12, pp. 1013–1015, Jun. 1994.

[16] A. Ortiz-Conde, F. J. García-Sánchez, and J. J. Liou, "An improved method for extracting the difference between drain and source resistances in MOSFETs," *Solid-State Electron.*, vol. 39, no. 3, pp. 419–421, Mar. 1996.

[17] A. Ortiz-Conde, J. J. Liou, R. Narayanan, and F. J. García-Sánchez, "Determination of physical mechanism contributing to the difference between drain and source resistances in short-channel MOSFETs," *Solid-State Electron.*, vol. 39, no. 2, pp. 211–215, Feb. 1996.

[18] A. Raychaudhuri, M. J. Deen, M. I. H. King, and J. Kolk, "Finding the asymmetric parasitic source and drain resistances from the AC conductances of a single MOSFET," *Solid-State Electron.*, vol. 39, no. 6, pp. 909–913, Jun. 1996.

[19] H. Bae *et al.*, "Extraction of separated source and drain resistances in amorphous indium-gallium-zinc oxide TFTs through C-V characterization," *IEEE Electron Device Lett.*, vol. 32, no. 6, pp. 761–763, Jun. 2011.

[20] F. Torricelli, M. Ghittorelli, L. Colalongo, and Z. M. Kovács-Vajna, "Single-transistor method for the extraction of the contact and channel resistances in organic field-effect transistors," *Appl. Phys. Lett.*, vol. 104, no. 9, Mar. 2014, Art. no. 093303.

[21] A. Tsormpatzoglou *et al.*, "Analytical surface-potential-based drain current model for amorphous InGaZnO thin film transistors," *J. Appl. Phys.*, vol. 114, no. 18, Nov. 2013, Art. no. 184502.

[22] H. He and X. Zheng, "Analytical model of undoped polycrystalline silicon thin-film transistors consistent with Pao–Sah model," *IEEE Trans. Electron Devices*, vol. 58, no. 4, pp. 1102–1107, Apr. 2011.

[23] N. Arora, *MOSFET Models for VLSI Circuit Simulation: Theory and Practice*. New York, NY, USA: Springer-Verlag, 1993.

[24] A. Valletta *et al.*, "Contact effects in amorphous InGaZnO thin film transistors," *J. Display Technol.*, vol. 10, no. 11, pp. 956–961, Nov. 2014.

[25] F. Yu, X. Ma, W. Deng, J. J. Liou, and J. Huang, "A surface-potential-based drain current compact model for a-InGaZnO thin-film transistors in non-degenerate conduction regime," *Solid-State Electron.*, vol. 137, pp. 38–43, Nov. 2017.

[26] S. Lee *et al.*, "Trap-limited and percolation conduction mechanisms in amorphous oxide semiconductor thin film transistors (TFTs)," *Appl. Phys. Lett.*, vol. 98, no. 20, May 2011, Art. no. 203508.

[27] M. Ghittorelli, F. Torricelli, and Z. M. Kovács-Vajna, "Analytical physical-based drain-current model of amorphous InGaZnO TFTs accounting for both non-degenerate and degenerate conduction," *IEEE Electron Device Lett.*, vol. 36, no. 12, pp. 1340–1343, Dec. 2015.

[28] J. Fang, W. Deng, X. Ma, J. Huang, and W. Wu, "A surface-potential-based DC model of amorphous oxide semiconductor TFTs including degeneration," *IEEE Electron Device Lett.*, vol. 38, no. 2, pp. 183–186, Feb. 2017.

[29] W.-J. Wu *et al.*, "Analytical extraction method for density of states in metal oxide thin-film transistors by using low-frequency capacitance-voltage characteristics," *IEEE/OSA J. Display Technol.*, vol. 12, no. 9, pp. 888–891, Sep. 2016.

[30] W. Deng, J. Fang, X. Wei, W. Wu, and J. Huang, "A core compact model for IGZO TFTs considering degeneration mechanism," *IEEE Trans. Electron Devices*, vol. 65, no. 4, pp. 1370–1376, Apr. 2018.

[31] A. Valletta *et al.*, "Contact effects in high performance fully printed P-channel organic thin film transistors," *Appl. Phys. Lett.*, vol. 99, no. 23, Dec. 2011, Art. no. 233309.

XIXIONG WEI received the B.S. degree from Jiangxi Science and Technology Normal University, Nanchang, China, in 2015, and the M.S. degree from Jinan University, Guangzhou, China, in 2018.

NA LI received the B.S. degree from the Hubei University of Education, Wuhan, China, in 2017. She is currently pursuing the M.S. degree with Jinan University, Guangzhou, China.

Her current research interest includes the modeling of the organic thin-film transistors.

WEIJING WU was born in Fuzhou, China. He received the Ph.D. degree from the South China University of Technology, Guangzhou, China, in 2008.

In 2008, he joined the Institute of Polymer Optoelectronic Materials and Devices, South China University of Technology, where he is currently an Associate Professor with the State Key Laboratory of Luminescent Materials and Devices. His current research interests include thin-film transistors and AMOLED displays.

WANLING DENG received the B.S. and Ph.D. degrees in electrical engineering from the South China University of Technology, Guangzhou, China, in 2003 and 2008, respectively.

Since 2008, she has been an Associate Professor with the Department of Electronic Engineering, Jinan University, Guangzhou. Her current research interests include thin-film transistor (TFT) devices and physics, particularly poly-Si TFT and AOS TFT modeling.

JUNKAI HUANG received the B.S. degree in applied physics and the M.S. degree in semiconductor device from Jinan University, Guangzhou, China, in 1985 and 1990, respectively, and the Ph.D. degree from the Institute of Microelectronics, South China University of Technology, Guangzhou, in 2011.

He is currently a Professor with Jinan University. His current research interests include thin-film transistors' modeling, simulation, and integrated circuit design.